remote sensing

MDPI

Letter

Using CYGNSS Data to Monitor China's Flood Inundation during Typhoon and Extreme Precipitation Events in 2017

Wei Wan [1], Baojian Liu [1], Ziyue Zeng [2], Xi Chen [1], Guiping Wu [3], Liwen Xu [1], Xiuwan Chen [1] and Yang Hong [1,4,*]

1 Institute of Remote Sensing and GIS, School of Earth and Space Sciences, Peking University, Beijing 100871, China; w.wan@pku.edu.cn (W.W.); liubaojian@pku.edu.cn (B.L.); chenxi928@pku.edu.cn (X.C.); liwenxu@pku.edu.cn (L.X.); xwchen@pku.edu.cn (X.C.)
2 Department of Hydraulic Engineering, Tsinghua University, Beijing 100084, China; ceng-14@mails.tsinghua.edu.cn
3 Nanjing Institute of Geography and Limnology, Chinese Academy of Sciences, Nanjing 210008, China; gpwu@niglas.ac.cn
4 School of Civil Engineering and Environmental Science, University of Oklahoma, Norman, OK 73019, USA
* Correspondence: yanghong588@pku.edu.cn; Tel.: +86-10-62744775

Received: 20 February 2019; Accepted: 3 April 2019; Published: 9 April 2019

Abstract: NASA's Cyclone Global Navigation Satellite System (CYGNSS) mission, launched in 2016, is a small satellite constellation designed to measure the ocean surface wind speed in hurricanes and tropical cyclones. To explore its additional capabilities for applications on the land surface, this study investigated the advantages and limitations of using CYGNSS data to monitor flood inundation during typhoon and extreme precipitation events in southeast China in 2017. The results showed that despite the lack of quantitative evaluation, the CYGNSS-derived surface reflectivity (SR) and flood inundation area was qualitatively consistent with the Global Precipitation Measurement (GPM)-derived precipitation and Soil Moisture Active Passive (SMAP)/Soil Moisture and Ocean Salinity (SMOS)-derived total brightness temperature at circular polarization (T_{bC}). The results provide supporting evidence for further designation of Global Navigation Satellite System (GNSS) reflectometry (GNSS-R) constellations to monitor land surface hydrology.

Keywords: CYGNSS; GNSS-R; flood inundation; typhoon; extreme precipitation

1. Introduction

Natural disasters occur frequently in China due to its complex geographic environment. Typhoons and extreme precipitation are two kinds of primary natural disasters, particularly occurring in southeast China along the coast and middle and lower Yangtze River [1]. Flood disaster risks induced by flooding events have been causing increasing concerns due to the dense population and highly developed economies in these regions [2].

The timely and accurate mapping of the areas most impacted by flooding events can reinforce the capacity building of emergency response teams when disasters occur. Satellite remote sensing is an effective approach to mapping flooded regions [3]. However, optical remote sensing (e.g., Moderate Resolution Imaging Spectroradiometer (MODIS) and Landsat) does not work during flood events due to the influence of clouds and rain. Microwave remote sensing, in contrast, is not affected by severe weather. However, microwave observations are either at coarse spatial resolutions (10–70 km for passive sensors, e.g., Soil Moisture Active Passive (SMAP), Soil Moisture and Ocean Salinity (SMOS), Scanning Multi-channel Microwave Radiometer (SMMR) and Advanced Microwave

Scanning Radiometer - Earth Observing System (AMSR-E)) or temporal resolutions (6–16 days for Synthetic Aperture Radar (SAR), e.g., TerraSAR-X, Advanced Land Observing Satellite-2 (ALOS-2), and Sentinel-1 SAR).

The Global Navigation Satellite System Reflectometry (GNSS-R) is a bistatic radar approach to infer surface properties through analyzing the L band-reflected GNSS signals over the Earth's surface. This technique is cost-effective since it uses operational GNSS satellites as microwave transmitters. Compared to monostatic radar, which measures backscattered signals, this technique is less sensitive to surface roughness since it measures the forward-scattered GNSS signals from the surface [4]. Since the launch of NASA's Cyclone GNSS (CYGNSS) mission in 2016, spaceborne GNSS-R has revealed its potential to observe ocean/land surfaces at a fine spatial (from a few kilometers to tens of kilometers) and temporal (from a few hours to 1–3 days) resolution [5,6]. CYGNSS is a constellation consisting of eight small satellites carrying GNSS receivers specially designed to capture surface-reflected GNSS signals over the tropics to retrieve ocean surface wind speeds. To explore additional capabilities, previous studies have shown initial applications to monitor land surface hydrological components such as soil moisture [7,8], lake ice thickness/water levels [9,10], and wetlands [11]. The first attempt, described in [6], used CYGNSS data to map flood inundation during the 2017 Atlantic hurricane season.

This paper presents the advantages and limitations of using CYGNSS data to monitor flood inundation during typhoons and extreme precipitation events of 2017 in southeast China. The results show the capability of CYGNSS for both monitoring flood inundation dynamics and acquiring flood inundation areas. The primary methodologies for processing CYGNSS data and SMOS/SMAP data in this study were similar to those used in [6,12], and the results further consolidate the conclusions presented in [6,12]. This work provides supporting evidence for the further use of GNSS-R constellations to monitor land surface hydrology.

2. Materials and Methods

2.1. Data

There were eight typhoon events and two extreme precipitation events in China during 2017 [1]. Since most typhoon events in southeast China occur from July to September, in this study we defined a typhoon season as ranging from the first typhoon event in July to the last typhoon event in September, i.e., Days of Year (DOYs) 202–253. There were six typhoon events during the defined typhoon season (Table 1 and Figure 1a1), which are analyzed in Section 3.1. Note that two typhoon events, Nasha and Haitang, occurred successively and were studied further as typical cases for monitoring the flood inundation dynamics in Section 3.2. Two extreme precipitation events also occurred in southeast China, i.e., one from 22 June–2 July, and the other from 11 August–14 August 2017. Considering the spatial coverage of the CYGNSS data, in this study we only analyzed the first event, see Section 3.3. The Poyang Lake basin, located in the middle of the worst-hit area of this event, was studied as a typical case for comparisons between flood inundation derived from CYGNSS data and that from other data sources.

The CYGNSS data used in this study were from level 1, version 2.0, available via https://podaac.jpl.nasa.gov/. Delay-Doppler maps (DDMs) were the main observable in the data. DDMs are created by cross-correlating the received surface-reflected signal with a locally generated replica for different path delays (resulting from the path distance between the transmitter, reflecting surface, and receiver) and Doppler shifts (resulting from the relative motions of the transmitter, reflecting surface, and receiver) [13]. It is defined as the power $P(\tau, f)$ of the correlator output as a function of the applied delay τ and Doppler f offsets with respect to reference [14]. The CYGNSS DDMs are made of 17 delay pixels by 11 Doppler pixels, with a Doppler resolution of 500 Hz and a delay resolution of 249.4 ns. Areas with a surface elevation higher than 600 m above sea level were masked out due to a limitation in the CYGNSS on-board data compression algorithm [5]. The data were then filtered for (1) a signal-to-noise ratio (SNR) of the peak DDM value greater than 5 dB (since there have been

uncertainties reported in the measured antenna gain patterns that increase with increasing distance from the peak of the main lobe [13]); and (2) the elevation angle of the specular points higher than 30° (to prevent multipath effects).

Table 1. The typhoon and extreme precipitation events of 2017 investigated in this study.

	Name	Landfall Time	Landfall Location	Maximum Wind Speed When Landing (m/s)
Typhoon	Luoke	Jul. 23	Hongkang (22.4 N, 114.3 E)	20
	Nasha	Jul. 29	Yilan, Taiwan (24.7 N, 121.8 E)	40
		Jul. 30	Fuqing, Fujian (25.5 N, 119.6 E)	33
	Haitang	Jul. 30	Pingdong, Taiwan (22.5 N, 120.5 E)	23
		Jul. 31	Fuqing, Fujian (25.5 N, 119.6 E)	18
	Tiange	Aug. 23	Zhuhai, Guangdong (22.0 N, 113.2 E)	45
	Paka	Aug. 27	Taishan, Guangdong (22.0 N, 113 E)	33
	Mawa	Sep. 3	Shanwei, Guangdong (22.9 N, 115.9 E)	20
Extreme precipitation	Southeast China (20–31 N, 100–122 E), lasting for 11 days from Jun. 22 (DOY 173) to Jul. 2 (DOY 183)			

To qualitatively compare to the CYGNSS-derived surface reflectivity (SR), which is the main method of monitoring flood inundation, in this study, the Integrated Multi-satelliE Retrievals for Global Precipitation Measurement (GPM IMERG) precipitation products (Level 3, daily, 10 km, downloaded from https://pmm.nasa.gov/) were used. To compare with the flood inundation area calculated from the CYGNSS SR, two types of brightness temperature (T_b) data, i.e., SMOS (Level 1C, ~1.4 GHz), and SMAP (Level 2, ~1.4 GHz) were used. All the T_b data were downloaded from the NASA National Snow and Ice Data Center (NSIDC). The 2015 land cover/use classification data of China with 1 km resolution was derived from http://www.resdc.cn/. The NASA Shuttle Radar Topographic Mission (SRTM) 90 m Digital Elevation Models (DEM) Database v4.1 were used to calculate the elevation of the CYGNSS covered areas.

2.2. Calculation of the Flood Inundation Area

The SR derived from CYGNSS is strongly linked to the hydrological conditions of the surface. Referring to the bistatic radar equation [15] and the methods proposed in [6], for each specular reflection point, the SR (in dB) was calculated from the SNR observation of the DDMs:

$$SR \propto SNR - 10\log P_r^t - 10\log G^t - 10\log G^r - 20\log \lambda + 20\log(R_{ts} + R_{sr}) + 20\log(4\pi) \quad (1)$$

where P_r^t is the transmitted power; G^t and G^r are the gains of the transmitting antenna and the receiving antenna respectively; λ is the GPS wavelength (0.19 m); R_{ts} is the distance between the transmitter and the specular reflection point; and R_{sr} is the distance between the specular reflection point and the receiver.

As shown in the CYGNSS metadata, the SNR (in dB) is defined as $10\log(S_{max}/N_{avg})$, where S_{max} is the maximum value (in raw counts, this means peak cross-correlation of the DDM) in a single DDM bin, and N_{avg} is the average per-bin raw noise counts. The value of the SNR is related to surface dielectric constant at the specular reflection point of the GNSS signal, and the dielectric constant can be related to the moisture content of the surface. Since SNR is not equal in magnitude to the reflected power, the observations and corrections made in Equation (1) result in magnitudes greater than 100 dB. In this study, for the SR to be in a range that visually makes sense [6], 115 dB was subtracted from the original SR. To calculate the flood inundation areas for SR, a simple threshold was used to distinguish water from non-water areas. We collected observations over known permanent waterbodies within the study area and took the average of these observed values over all time to determine the final threshold (i.e., 17 dB). This threshold was different from that used in [6] (i.e., 12 dB). More tests considering environmental conditions (e.g., vegetation cover, and roughness) should be performed if this method is used to obtain flooding information.

To provide consistency with the time series analysis, the original SRs of the specular points were converted to gridded data. Three types of grids with appropriate spatial scales were applied, considering the number of data points within the corresponding study area and time period, i.e., 10 km × 10 km for the SR of the entire typhoon/non-typhoon season over southeast China (Figure 1), 50 km × 50 km for the daily SR of Fujian and Taiwan (Figure 2), and 30 km × 30 km for the daily SR of the Poyang Lake basin (Figure 3). The data value per grid cell was determined as the average value of the specular points that dropped into the grid.

2.3. Conversion of the SMAP/SMOS-Derived Brightness Temperature

The brightness temperature T_b observed by microwave radiometers has been demonstrated to have strong differential responses to water and land [16], with lower T_b representing wetter land and vice versa. To compare this with CYGNSS data, it is better to use SMAP and SMOS data than other microwave radiometer data, since these two types of data have similar frequencies as that of the GPS L1 band (~1.58 GHz), therefore giving them similar sensitivities to surface conditions. The GNSS signals are circular polarization with a certain degree of ellipticity, while SMAP/SMOS measures the T_b at the two linear polarizations (H and V) [12]. To correlate the CYGNSS-derived SR with the SMAP/SMOS-derived T_b, the SMAP/SMOS-derived T_b was converted to total T_b at circular polarization using the following equation [12]:

$$T_{b_C} = \left(T_{b_H} + T_{b_V}\right)/2 \tag{2}$$

where T_{b_C} is the total T_b at circular polarization and T_{b_H} and T_{b_V} are the T_b at H and V linear polarizations, respectively.

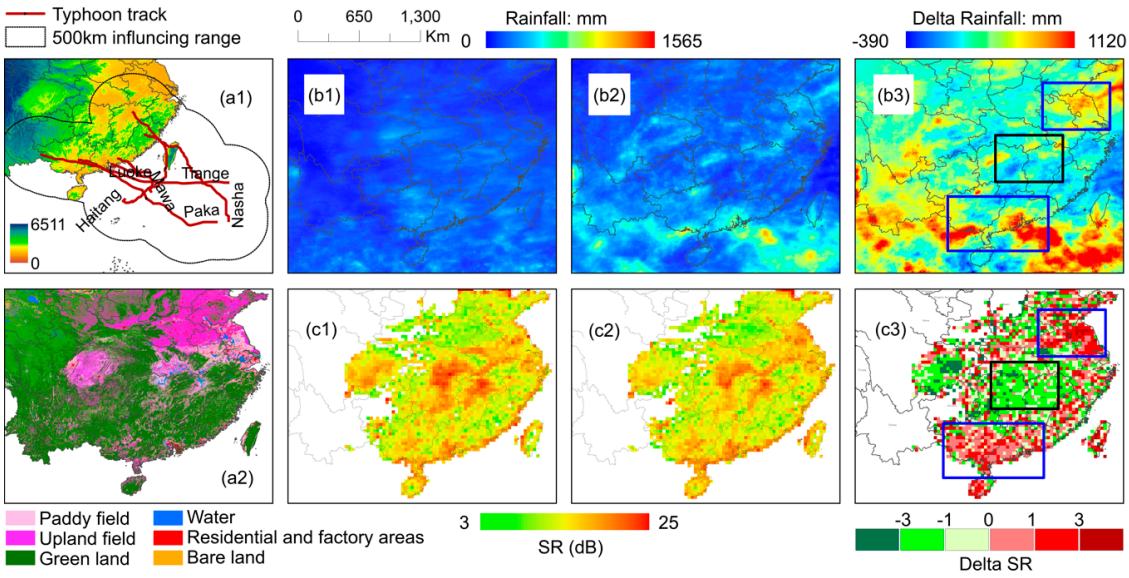

Figure 1. Precipitation (Global Precipitation Measurement (GPM)-derived) and surface reflectivity (SR) (Cyclone Global Navigation Satellite System (CYGNSS)-derived) changes of southeast China during the 2017 typhoon season. (**a1**) Typhoon tracks; the background map is the NASA Shuttle Radar Topographic Mission (SRTM) 90 m digital elevation models (DEM), and the black line represents the 500 km influencing range of the typhoon [18]; (**a2**) Land cover/use classification; (**b1**–**b3**) Precipitation of non-typhoon season and typhoon season and their differences (Delta rainfall); (**c1**–**c3**) SR of non-typhoon season and typhoon season and their differences (Delta SR). Blue and black boxes (**b3**,**c3**) represent regions with positive and negative delta SRs, respectively. SR: Surface reflectivity.

3. Results and Discussion

3.1. Overall Evaluations during the Typhoon Season

To evaluate the influence of the entire typhoon season, a non-typhoon season, i.e., DOY 99–150 was defined with the same interval of time as the typhoon season, starting from the available date of the CYGNSS data. Figure 1 shows the change of precipitation (GPM-derived, b1–b3) and SR (CYGNSS-derived, c1–c3) over southeast China before and after the 2017 typhoon season. The accumulated SRs of the non-typhoon and typhoon seasons were gridded into a 10 km resolution. There was no significant correlation when directly comparing the values of precipitation and the SR (Figure 1). However, note that the differences of the SRs (typhoon minus non-typhoon, see Figure 1c3) were positive over the northeast and south of this region (see blue boxes), while they were negative over the middle of the region, which is the Yangtze River basin (see black box). This phenomenon is consistent with the differences in precipitation shown in Figure 1b3. Additionally, the terrain of the middle coast is relatively high (see Figure 1a1), which could prevent the wind and rain from passing through to inland areas. For some paddy fields within the Yangtze River basin (Figure 1a2), higher SRs were observed during the non-typhoon season than during the typhoon season. This is likely due to the high water coverage during the rice transplanting period and the vegetation attenuation of the GPS L band microwave signal during the growing period [17].

3.2. Flood Inundation During Typhoon Events Nasha and Haitang

Nasha and Haitang were two successive typhoon events that occurred on 29–31 July 2017. These two events brought great disasters mainly to two provinces of China, Fujian and Taiwan. Figure 2 shows the daily variations of precipitation (GPM-derived, b1–b5), SR (CYGNSS-derived, c1–c5) and the inundated areas of Fujian and Taiwan (SR-derived, d1–d5) during and after the typhoon events. Since the available specular points of the daily CYGNSS data are sparse, the SR and inundated areas are gridded into 50 km resolution.

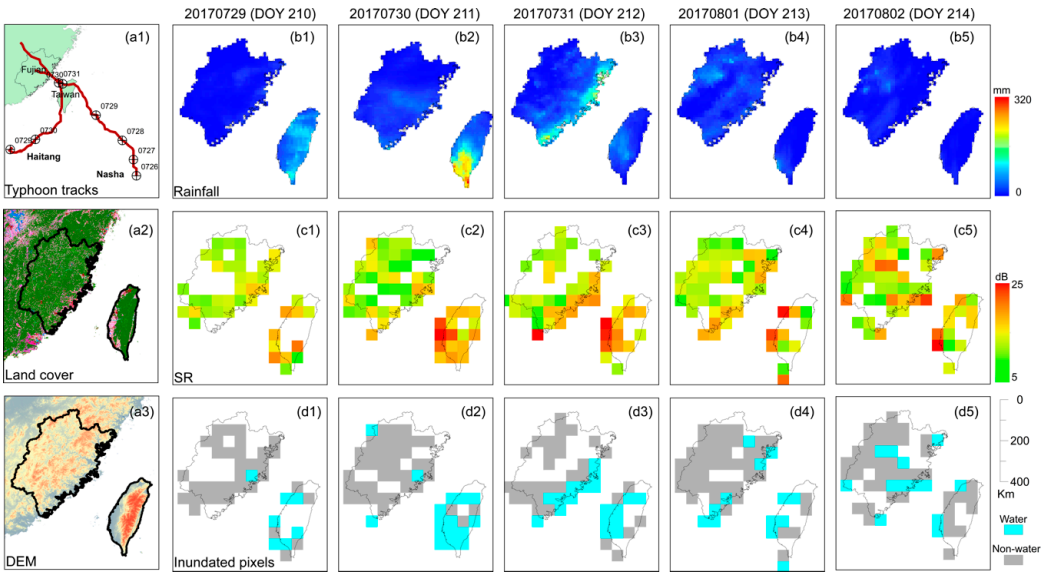

Figure 2. Daily variations of precipitation (**b1–b5**), GPM-derived)), SR (**c1–c5**), CYGNSS-derived)), and inundated area (**d1–d5**), SR-derived)) of Fujian and Taiwan during Typhoons Nasha and Haitang. SR: Surface reflectivity.

In general, the precipitation and SR had consistent change patterns during the events. Note that the change of SR was consistent with that of typhoon rainfall, particularly on 30 July 2017, when there was extreme accumulated rainfall of up to 320 mm in south Taiwan. There are also inconsistencies

between SR and the precipitation, e.g., high SR values (Figure 2c4,c5 but low precipitation values (Figure 2b4,b5 over the west coast of Taiwan on 1 August and 2 August 2017. Vegetation cover (as shown in Figure 2a2) could attenuate the CYGNSS signals over the entire region to result in a relatively lower SNR than that of bare soil.

3.3. Flood Inundation in Poyang Lake Basin During the Extreme Precipitation Event

The extreme precipitation event investigated in this study affected the middle and lower reaches of the Yangtze River from 22 June to 2 July 2017 [1], with cumulative rainfall exceeding 500 mm in some areas. The event caused widespread regional and basin flooding as well as secondary geological disasters. To show its detailed characterization in CYGNSS data, we analyzed the data covering the northern part of the Poyang Lake basin, which is located in the middle of the worst-hit area. Figure 3 shows the SR (CYGNSS-derived) and the inundated areas (d1, d2) of this region during DOY 137 (before the event) and DOY 182 (the end of the event). The SRs are shown in two forms, i.e., scatters of the specular reflection (b1, b2) and 30 km gridded images (c1, c2). Note that the event caused flood inundation in the middle of the Poyang Lake basin, mostly covering the Ganjiang, Fuhe, Xinjiang, and regions around the lake. The coverage of the inundated area is also consistent with the DEM of this region (Figure 3a).

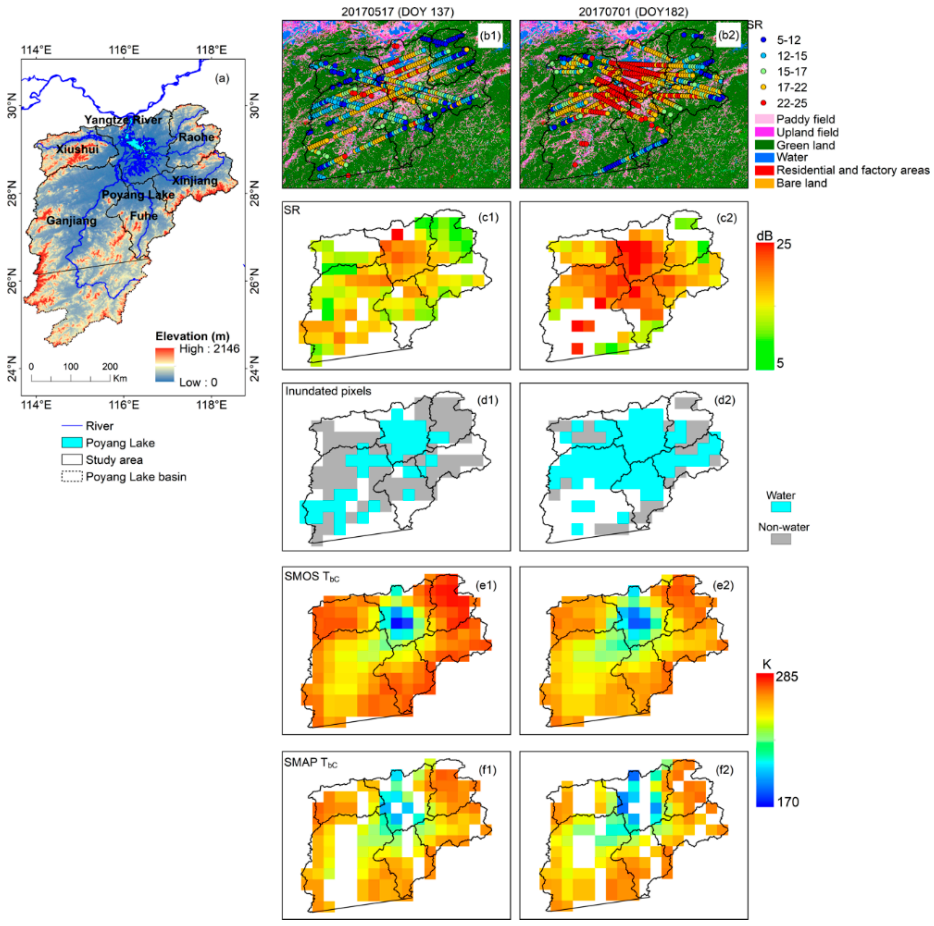

Figure 3. The CYGNSS-derived SR (**b1**,**b2**) and inundated areas (**c1**,**c2**) of the northern Poyang Lake Basin during Day of Year (DOY) 137 (before the event) and DOY 182 (the end of the event). (**a**) The Poyang Lake basin; (**e1**,**e2**) Soil Moisture and Ocean Salinity (SMOS) T_{bc}; (**f1**,**f2**) Soil Moisture Active Passive (SMAP) T_{bc}. SR: Surface reflectivity; T_{bc}: Total brightness temperature at circular polarization.

Figure 3e1,e2,f1,f2 show the characteristics of SMOS- and SMAP-derived T_{bc} (also gridded to 30 km) for the two corresponding dates, respectively. Due to the coverage limitations of the SMOS and

SMAP data, both the descending and ascending passes were used for these two dates. Qualitatively, Figure 3 shows that the SR and its resulting inundated area are consistent with the T_{b_C} maps. Figure 4 further compares pixel-wise values of CYGNSS SR and SMOS/SMAP T_{b_C} for DOY 137 and DOY 182 respectively. Overall, the Pearson correlation coefficients of SR vs. SMOS T_{b_C} ($R = -0.66$ for DOY 137 and $R = -0.70$ for DOY 182) are almost the same as that of SR vs. SMAP T_{b_C} ($R = -0.66$ for DOY 137 and $R = -0.71$ for DOY 182).

The correlations between SR and T_{b_C} are shown in Figure 4 as a function of (a, b) soil moisture and (c, d) nadir vegetation opacity. The nadir vegetation opacity is an indicator of the attenuation of the electromagnetic signal through the vegetation layer. It showed a dynamic range of 0~0.6 cm^3/cm^3 for soil moisture along the complete SR dynamic range, while T_{b_C} appeared saturated at ~270 K with nadir vegetation opacity values of ~0.7. Similar to results shown in [19] over inundated wetlands, this indicates that CYGNSS data (which is forward scattering) are less affected by vegetation cover over inundated regions. This phenomenon is also consistent with results shown in [12] for Thailand, since these two regions have similar land surface conditions (i.e., cropland with high soil moisture, high-to-moderate vegetation, and moderate-to-low land cover heterogeneity). The threshold (SR = 17 dB) for extracting the flood inundation area is also shown in each subfigure of Figure 4 (see black dashed line). Note that on DOY 182 (the end of the event), most pixels with low T_{b_C} and high soil moisture could be correctly identified as inundated pixels. This indicates that flood water was the major contributor to the high SR, while effects from vegetation were relatively low. However, on DOY 137 (before the event), pixels with low T_{b_C}, high soil moisture and high vegetation opacity could not be correctly identified as 'water' pixels, particularly for those SMAP pixels (see red triangles in (a) and their corresponding triangles in (c) in Figure 4). This indicates that vegetation attenuation on SR was nonnegligible at this stage.

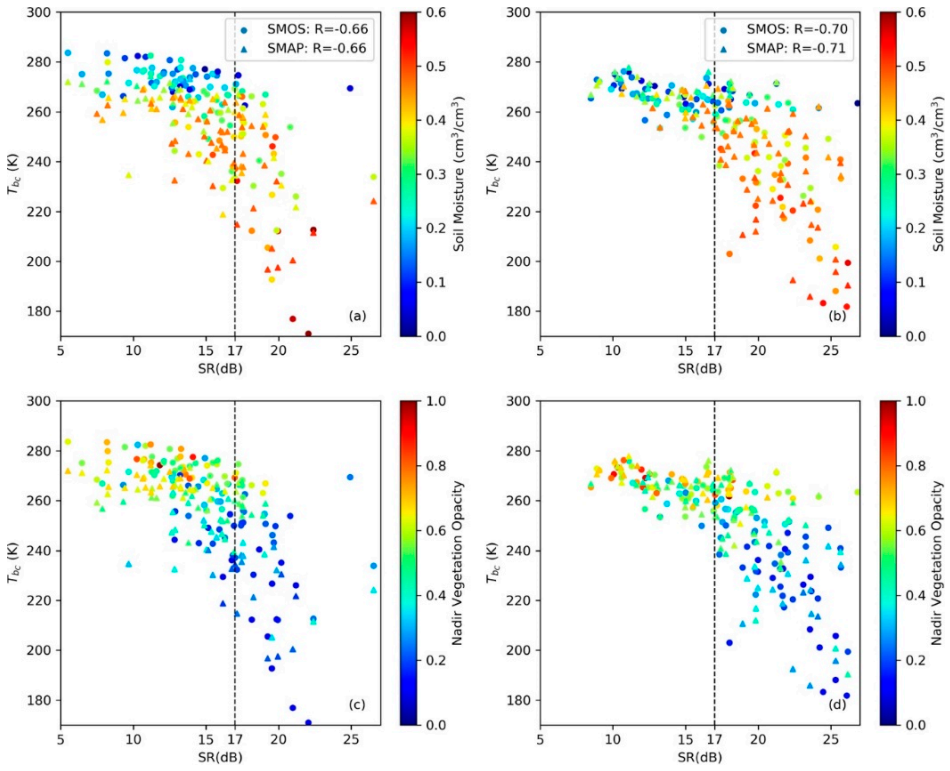

Figure 4. Correlations between CYGNSS SR and SMOS/SMAP T_{b_C} for (**a**,**c**) DOY 137 and (**b**,**d**) DOY 182 respectively, as a function of (**a**,**b**) soil moisture and (**c**,**d**) nadir vegetation opacity. Black dashed line: threshold (SR = 17 dB) for extracting flood inundation area; SR: Surface reflectivity; T_{b_C}: Total brightness temperature at circular polarization.

3.4. Limitations of the Data and Methods

The CYGNSS small satellite constellation has proposed a new paradigm in earth environmental monitoring due to its unique data acquiring mechanism [5]. For monitoring flooding over land, as shown in this study, it is able to reach a high temporal resolution, i.e., at a daily scale. However, as shown in Figure 2, it could not guarantee a high spatial resolution for inundation mapping in regions with moderate-to-high topography and surface roughness [6]. Using the spaceborne GNSS-R technique, through the design of new constellations for monitoring land rather than ocean, e.g., constellations with more small satellites and better data transmission approaches, the spatial and temporal resolution of this technique will be greatly improved.

The methods used in this study have several limitations: (1) this study used the version 2.0 CYGNSS data, and the newly released version 2.1 data could be used to derive a better-calibrated SNR; (2) the simple threshold to isolate water and land is not universal. Calibration should be performed to produce flood products using CYNGSS data or data in future GNSS-R missions; (3) gridding the daily CYGNSS data to 30 km or 50 km is likely inappropriate as it will grossly overestimate the actual extent of flooding.

4. Conclusions

In summary, this study proposed to use CYGNSS data to monitor the occurrence of floods in China during the typhoon and extreme precipitation events of 2017. The SR calculated from CYGNSS DDM SNR was used as the main observable to extract the flood inundation area. The CYGNSS-derived flood inundation area was qualitatively consistent with the GPM-derived precipitation and SMAP/SMOS-derived T_{b_C}. Despite the lack of quantitative evaluation, the results of this study further consolidate the conclusions presented in previous studies. In addition to its primary objective, which was the measurement of ocean surface wind speeds in hurricanes and tropical cyclones, the CYGNSS constellation was demonstrated to have potential in monitoring flood dynamics triggered by typhoon and extreme precipitation events with high temporal resolution. With the further development of the payload and models, more spaceborne GNSS-R data (e.g., CYGNSS follow-on, Cookie [20,21]) will be acquired in the near future with higher spatial/temporal resolution and higher quality, and this improvement could bring more potential applications in land surface hydrology.

Author Contributions: Conceptualization, W.W., X.C. (Xiuwan Chen) and Y.H.; methodology, W.W., B.L., Z.Z., X.C. (Xi Chen) and L.X.; validation, G.W. and Z.Z.; formal analysis, W.W., B.L., X.C. (Xi Chen) and L.X.; resources, Y.H.; writing—original draft preparation, W.W.; writing—review and editing, Y.H., Z.Z. and B.L.; supervision, Y.H. and X.C. (Xiuwan Chen); funding acquisition, W.W. and Y.H.

Funding: This study is financially supported by the Key R&D Program of the Ministry of Science and Technology, China (Grant No. 2018YFC1506504). The work related to CYGNSS data processing is supported by the National Natural Science Foundation of China (NSFC) project (Grant No. 41501360).

Acknowledgments: The first author is grateful to Wan'er Zhao for her contributions to the text writing of this manuscript.

Conflicts of Interest: The authors declare no conflict of interest. The funding sponsors had no role in the design of the study, in the collection, analyses, or interpretation of data, in the writing of the manuscript, and in the decision to publish the results.

References

1. China Meteorological Administration. *China Climate Bulletin 2017*; China Meteorological Administration: Beijing, China, 2017; pp. 30–33.
2. Zhang, Q.; Gu, X.; Singh, V.P.; Shi, P.; Luo, M. Timing of floods in southeastern China: Seasonal properties and potential causes. *J. Hydrol.* **2017**, *552*, 732–744. [CrossRef]
3. Klemas, V. Remote Sensing of Floods and Flood-Prone Areas: An Overview. *J. Coast. Res.* **2014**, 1005–1013. [CrossRef]

4. Masters, D.; Axelrad, P.; Katzberg, S. Initial results of land-reflected GPS bistatic radar measurements in SMEX02. *Remote Sens. Environ.* **2004**, *92*, 507–520. [CrossRef]
5. Ruf, C.S.; Chew, C.; Lang, T.; Morris, M.G.; Nave, K.; Ridley, A.; Balasubramaniam, R. A New Paradigm in Earth Environmental Monitoring with the CYGNSS Small Satellite Constellation. *Sci. Rep.* **2018**, *8*, 8782. [CrossRef] [PubMed]
6. Chew, C.; Reager, J.T.; Small, E. CYGNSS data map flood inundation during the 2017 Atlantic hurricane season. *Sci. Rep.* **2018**, *8*, 9336. [CrossRef] [PubMed]
7. Chew, C.C.; Small, E.E. Soil Moisture Sensing Using Spaceborne GNSS Reflections: Comparison of CYGNSS Reflectivity to SMAP Soil Moisture. *Geophys. Res. Lett.* **2018**, *45*, 4049–4057. [CrossRef]
8. Kim, H.; Lakshmi, V. Use of Cyclone Global Navigation Satellite System (CyGNSS) Observations for Estimation of Soil Moisture. *Geophys. Res. Lett.* **2018**, *45*, 8272–8282. [CrossRef]
9. Li, W.; Cardellach, E.; Fabra, F.; Ribó, S.; Rius, A. Lake Level and Surface Topography Measured With Spaceborne GNSS-Reflectometry From CYGNSS Mission: Example for the Lake Qinghai. *Geophys. Res. Lett.* **2018**. [CrossRef]
10. Mayers, D.; Ruf, C. Measuring Ice Thickness with Cygnss Altimetry. In Proceedings of the 2018 IEEE International Geoscience and Remote Sensing Symposium, Valencia, Spain, 22–27 July 2018; pp. 8535–8538.
11. Lavalle, M.; Morris, M.; Shah, R.; Zuffada, C.; Nghiem, S.V.; Chew, C.; Zavorotny, V.U. Bistatic Scattering Modeling for Dynamic Mapping of Tropical Wetlands with Cygnss. In Proceedings of the 2018 IEEE International Geoscience and Remote Sensing Symposium, Valencia, Spain, 22–27 July 2018; pp. 239–242.
12. Carreno-Luengo, H.; Luzi, G.; Crosetto, M. Sensitivity of CyGNSS Bistatic Reflectivity and SMAP Microwave Radiometry Brightness Temperature to Geophysical Parameters Over Land Surfaces. *IEEE J. Sel. Top. Appl. Earth Obs. Remote Sens.* **2019**, *12*, 107–122. [CrossRef]
13. Chew, C.; Shah, R.; Zuffada, C.; Hajj, G.; Masters, D.; Mannucci, A.J. Demonstrating soil moisture remote sensing with observations from the UK TechDemoSat-1 satellite mission. *Geophys. Res. Lett.* **2016**, *43*, 3317–3324. [CrossRef]
14. Rius, A.; Cardellach, E.; Fabra, F.; Li, W.; Ribó, S.; Hernández-Pajares, M. Feasibility of GNSS-R Ice Sheet Altimetry in Greenland Using TDS-1. *Remote Sens.* **2017**, *9*, 742. [CrossRef]
15. Roo, R.D.D.; Ulaby, F.T. Bistatic specular scattering from rough dielectric surfaces. *IEEE Trans. Antennas Propag.* **1994**, *42*, 220–231. [CrossRef]
16. Van Dijk, A.I.J.M.; Brakenridge, G.R.; Kettner, A.J.; Beck, H.E.; De Groeve, T.; Schellekens, J. River gauging at global scale using optical and passive microwave remote sensing. *Water Resour. Res.* **2016**, *52*, 6404–6418. [CrossRef]
17. Wan, W.; Larson, K.M.; Small, E.E.; Chew, C.C.; Braun, J.J. Using geodetic GPS receivers to measure vegetation water content. *GPS Solut.* **2015**, *19*, 237–248. [CrossRef]
18. Khouakhi, A.; Villarini, G.; Vecchi, G.A. Contribution of Tropical Cyclones to Rainfall at the Global Scale. *J. Clim.* **2016**, *30*, 359–372. [CrossRef]
19. Nghiem, S.V.; Zuffada, C.; Shah, R.; Chew, C.; Lowe, S.T.; Mannucci, A.J.; Cardellach, E.; Brakenridge, G.R.; Geller, G.; Rosenqvist, A. Wetland monitoring with Global Navigation Satellite System reflectometry. *Earth Space Sci.* **2017**, *4*, 16–39. [CrossRef] [PubMed]
20. Norris, R.; Ruf, C.; Loria, E.; Brien, A.O. Comparison of Wide Bandwidth Conventional and Interferometric GNSS-R Techniques for Possible CYGNSS Follow-On Mission. In Proceedings of the 2018 IEEE International Geoscience and Remote Sensing Symposium, Valencia, Spain, 22–27 July 2018; pp. 4277–4280.
21. Martín-Neira, M.; Li, W.; Andrés-Beivide, A.; Ballesteros-Sels, X. "Cookie": A Satellite Concept for GNSS Remote Sensing Constellations. *IEEE J. Sel. Top. Appl. Earth Obs. Remote Sens.* **2016**, *9*, 4593–4610. [CrossRef]